Int. J. Electrochem. Sci., 7 **(2012)** 8905 - 8928

International Journal of
ELECTROCHEMICAL
SCIENCE
www.electrochemsci.org

Electrocatalytic Oxidation of Alcohols at Gold Electrodes in Alkaline Media

María Soledad Ureta-Zañartu[1,*], *Cristhian Berríos*[1], *Thaís González*[1], *Francisco Fernández*[1], *Daniela Báez*[1], *Ricardo Salazar*[1], *Claudio Gutiérrez*[2]

[1] Departamento de Ciencias del Ambiente, Facultad de Química y Biología, Universidad de Santiago de Chile, C. Libertador Bernardo O'Higgins 3363, Estación Central, Santiago, Chile.
[2] Instituto de Química Física "Rocasolano", CSIC, C. Serrano, 119, 28006-Madrid, Spain
[*]E-mail: soledad.ureta@usach.cl

Received: 14 June 2012 / *Accepted:* 28 July 2012 / *Published:* 1 September 2012

The electrooxidation in a pH 11 carbonate/hydrogen carbonate buffer of an aromatic (benzyl alcohol (*BA*)) alcohol and of several aliphatic alcohols on massive gold and on gold/quartz electrodes has been studied by cyclic voltammetry (*CV*), electrochemical impedance spectroscopy (EIS) and electrochemical quartz crystal microbalance (*EQCM*). The activity of gold is high for BA, lower for ethylene glycol (EG), and very low for propanol and butanol. Based on the fact that the double-layer capacity with BA is about one third of that for the aliphatic alcohols, which points to an expulsion of water from the Au surface due to the hydrophobic character of BA, we suggest that BA removes water molecules from the electrode surface, this removal facilitating its electrooxidation. The electrooxidation of BA started at the same potential, at -0.1 V, at which a surface redox process, corresponding to the adsorption-desorption of OH, appeared in the cyclic voltammogram of gold in the pH 11 buffer at higher temperatures, which indicates that the oxidation of BA occurs by its reaction with surface OH groups, in spite of their very low coverage at room temperature. BA adsorbs on Au, as shown by the EQCM: when BA was added to the cell while the Au/Q electrode was held at -0.2 V, no mass change was observed with 4.3 mM BA, while with 23.3 mM BA the mass increased by 70 ng cm^{-2}. The fairly high activity of Au for EG electrooxidation is attributed to the presence of two OH groups in the molecule. For the monohydroxylic alcohols the activity increases in the order ethanol< propanol<butanol, which we attribute to an increasing hydrophobic character that would facilitate the displacement of water molecules from the interface. The apparent activation energy for the oxidation of 2-propanol on Au was 45 kJ mol^{-1}, while that for ethylene glycol was only 30 kJ mol^{-1}, probably because the presence of two OH groups in the molecule facilitates its oxidation. Benzaldehyde was detected by HPLC as the main product of BA electrooxidation, reaching a maximum concentration at 10 min, at which the faradaic efficiency was 39%. At longer times the concentration of benzaldehyde decreased, probably because of its oxidation to benzoic acid.

Keywords: alcohol electro-oxidation; gold electrode; cyclic voltammetry; EQCM; EIS.

1. INTRODUCTION

The electro-oxidation of small alcohols has long been studied, mainly because of their possible use in fuel cells. Methanol, although extensively used, is rather toxic [1], and ethanol and ethylene glycol can easily be obtained from sugar and biomass [2-4]. The mechanism of the electrooxidation of alcohols on Pt is far from clear [5]. In acidic media, even small molecules such as ethanol yield intermediate oxidation products, typically aldehydes and carboxylic acids [6]. Recently, Colle et al. [7] reported that the C-C bond in ethanol can be broken using Pt stepped surfaces partially covered by tin adatoms.

Although on gold the formation of adsorbed OH, a powerful oxidation agent, is favoured in alkaline media [8], these have been avoided due to carbonation of the solution and the lack of a suitable membrane [9]. Novel electrodes modified with gold nanoparticles circumvent this problem [10]. Previous work has shown that in a pH 11 buffer ethylene glycol is oxidized at gold, while methanol is basically not [11]. Recently alkaline media have been tested for the oxidation of alcohols on noble metals [12]. It has been argued that in gold a range of non-equilibrium states lead to the formation of active sites on the gold surface [13,14]. Recently Gobal *et al.* [15] postulated that adsorbed OH is the active species in the oxidation of methanol on nickel electrodes, which would not be mediated by the Ni(II)/Ni(III) couple, as had long been accepted. Borkowska *et al.* [16] reported that gold electrodes prepared from a gold amalgam had a higher activity for methanol oxidation than smooth poly- and single-crystal gold electrodes, which they attributed to a higher OH adsorption.

Lai *et al.* [17] reported that the electrooxidation of ethanol at Pt and Au electrodes increased significantly at pH's higher than 10. Kutz *et al.* [18], using isotope labeling and sum-frequency generation spectroscopy, reported that in 0.1 M NaOH the oxidation of ethanol at a Pt electrode occurs with C-C bond cleavage and CO formation as early as 0.05 V (RHE), and that CO is oxidized at 0.45 V (RHE), a potential 0.2 V lower than that in acidic media.

Liang *et al.* [19] found that in 1 M KOH the final product of ethanol oxidation at Pd electrodes was the acetate anion, acetaldehyde being an active intermediate.

The oxidation of benzyl alcohol at gold electrodes has been little studied. Motheo *et al.* [20] used a nickel oxy-hydroxide electrode in alkaline media, obtaining benzoic acid as main oxidation product. Also using nickel/nickel hydroxide electrodes, Vijayabarathi *et al.* [21] found that, in 0.1 M KOH, in water the main oxidation product of aromatic primary alcohols was the corresponding aromatic carboxylic acid, but that in 67% *ter*-butanol + 33% water mixtures the main product was the corresponding aromatic aldehyde.

In the present work we have studied the oxidation of small aliphatic alcohols and of benzyl alcohol at bare gold electrodes in a weakly alkaline medium (so as to avoid Cannizzaro's reaction), in order to determine the effect of the aromaticity of the alcohol.

2. EXPERIMENTAL

Benzyl alcohol (BA), NaOH, $NaHCO_3$, and Na_2CO_3 were p.a. from Merck, and the aliphatic alcohols from Sigma-Aldrich. The solutions were freshly prepared with deionized, twice-distilled water and deaerated with N_2. A pH 11 carbonate/hydrogen carbonate buffer was the usual support electrolyte, although in some experiments 0.1 M NaOH was used. Usually the electrode was introduced in the BA solution at open circuit, unless otherwise specified.

Three types of working electrode were used: (1) screen-printed gold BT 220 (3.8 mm diameter, DropSens), (2) gold disc (2 mm diameter, CH Instruments), and (3) 10-MHz Au-covered AT-cut quartz electrode (Elchema), with a geometric area of 0.25 cm^2, a resonant area of 0.24 cm^2, a roughness factor of 2.35 (evaluated using the gold reduction charge from 0.473 to 0.141 V *vs*. Ag/AgCl, taking 400 $\mu C\ cm^{-2}$ for the reduction of a monolayer of AuO [22]) , and a constant of 4.4 ng $Hz^{-1}\ cm^{-2}$. The gold disc electrodes were polished with 0.1 μm alumina powder and sonicated for 10 min. A Pt helix of high area was the counter electrode, and a KCl-saturated Ag/AgCl electrode, connected to the cell by a Luggin capillary, was the reference. In the experiments at controlled temperature the reference electrode was used in a nonisothermal way [23]. Cyclic Voltammetry (CV) with simultaneous mass recording with the Electrochemical Quartz Crystal Microbalance (EQCM) (Elechema EQCN-501) was used. Unless otherwise stated, current densities have been referred to the geometric area.

Impedance measurements at constant potential were carried out at room temperature with a CHI 660C Electrochemical Work Station, using a 5mV rms sinusoidal modulation in the 10 kHz–10 mHz frequency range. The frequency was decreased in a logarithmic mode with 10 steps per decade over a total time of about 30 min, during which no significant impedance changes were observed. The impedance results were evaluated using the Nova 1.7 software from Autolab.

In order to determine the reaction products electrolyses at constant potential, with continuous magnetic stirring, in a three-compartment cell (35 mL working electrode compartment) were carried out with a gold foil of 2 cm^2 geometric area (both sides). Samples were analyzed by high-performance liquid chromatography (*HPLC*) HITACHI with a LaChrom Elite Diode Array Detector (DAD) with a wavelength range of 200-600 nm, using a Hi-Bar® (250 mm x 4 mm) Purospher® Star RP-18e (5 μm) column and a mobile phase of methanol/pH 3.2 phosphate buffer (50/50, v/v) at a flow rate of 0.5 mL min^{-1}. The injection volume was 20 μL. Benzyl alcohol (206.1 nm, t_R 10.6 min), benzyl aldehyde (254 nm, t_R 16.0 min), and benzoic acid (229.6 nm, t_R 13.2 min) could be detected (t_R is the retention time). The products were determined by comparing their retention times with those of reference products, both pure and mixed.

3. RESULTS AND DISCUSSION

3.1. CVs and mass curves of an Au/Q electrode in pH 11 buffer electrolyte

Although the behavior in EQCM of gold has been already described [11,24-27], it can be affected by the gold pretreatment. Therefore, we will briefly describe the mass curve obtained simultaneously with the CV at 0.02 V s^{-1} in a pH 11 carbonate/hydrogen carbonate buffer (Figure 1). Six well-known regions can be distinguished in Figs. 1A, 1B, and 1C, namely: (1) double layer region, in which the mass decreases due to desorption of water and ions; (2) beginning of OH adsorption, with a mass increase of about 0.14 μg cm^{-2}; (3) surface gold oxide formation, corresponding to peak A1 in the CV, with a mass increase less sharp than that of OH adsorption; (4) passive region, with a small mass increase; (5) reduction of the surface gold oxides, corresponding to peak C1, with a sharp mass decrease (region 5), and (6) cathodic double layer region.

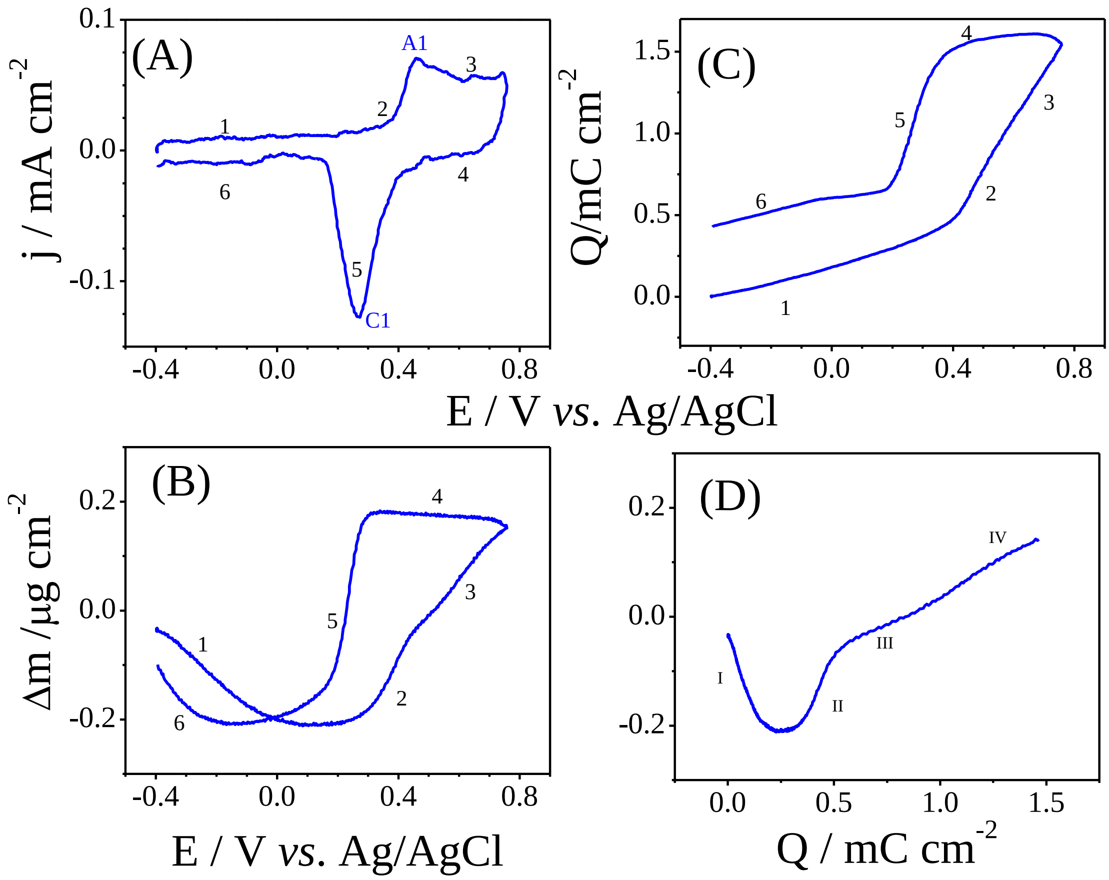

Figure 1. CVs and simultaneously recorded mass curves at 0.02 V s^{-1} of an Au/Q electrode in pH 11 buffer electrolyte: (A) Cyclic voltammogram. (B) Simultaneously recorded mass curve. (C) Electric charge obtained by integration of the CV in (A). (D) Plot of the mass change against the electric charge during the positive scan in (A). Roughness factor of the Au/Q electrode: 2.35.

With the help of the positive branch of the charge *vs.* potential curve given in Fig. 1C, the mass change *vs.* charge curve of Fig. 1D was obtained. In region I the mass decreases linearly with increasing positive charge of the double-layer capacitor, with a slope of about -1 mg C^{-1}. In region II of adsorbed OH formation the mass increases linearly with the charge, with a positive slope of 90 g / mol e$^-$, five times higher than that of 17 g/mol e$^-$ corresponding to the formation of OH. In region III of gold oxide formation a linear segment again obtains, with a positive slope of 21 g/mol e$^-$, 2.6 times higher than that of 8 g/mol e$^-$ expected for the formation of AuO. It is clear that in the three regions desorption/adsorption of anions and water control the mass changes.

3.2. Oxidation of alcohols by EQCM-CV techniques

3.2.1. CVs and mass curves at 0.1 V s^{-1} of benzyl alcohol and five aliphatic alcohols on Au/Q

The CVs and mass curves at 0.1 V s^{-1} of Au/Q in the pH 11 buffer electrolyte (thick solid curve) and with ethanol, 1- and 2-propanol, butanol and ethylene glycol at concentrations between 10 and 50 mM, and with benzyl alcohol at concentrations between 4.3 and 29.2 mM admitted at open circuit are given in Figure 2. The oxidation of BA yields an unsymmetric, very wide peak (A2) extending from -0.23 to 0.74 V (Fig. 2A). Although the maximum concentration of BA was smaller than that of the other alcohols, due to its smaller solubility in the pH 11 buffer, BA yielded the highest currents of all the alcohols tested.

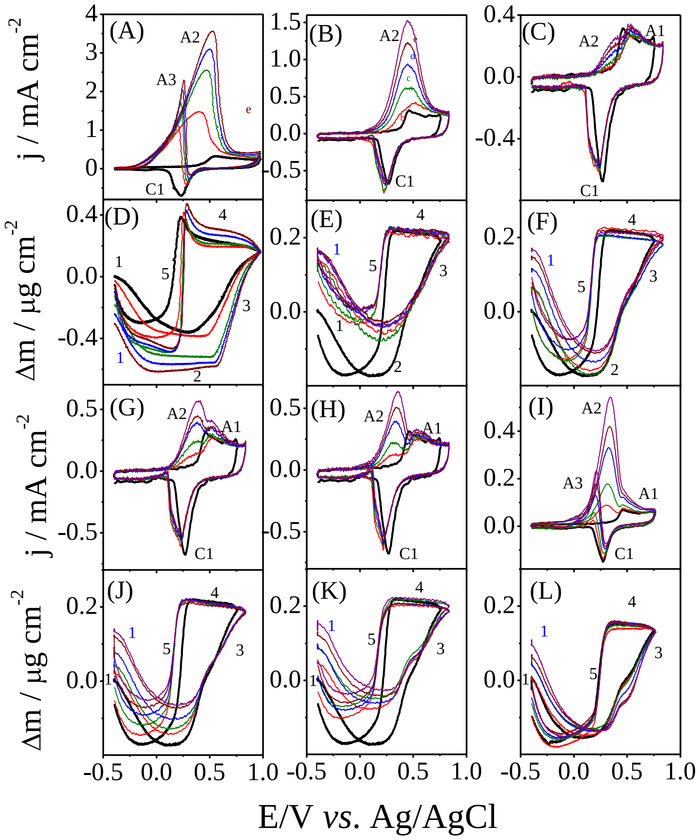

Figure 2. CVs and simultaneously recorded mass curves at 0.1 V s^{-1} of an Au/Q electrode in pH 11 buffer electrolyte (thick black line) and in the presence of: (A and D) 4.3-29.2 mM benzyl alcohol. (B and E) 10-50 mM ethylene glycol. (C and F) ethanol. (G and J)1-propanol. (H and K) 2-propanol. (I) and (L) also correspond to 2-propanol but at 0.02 V s^{-1}.

As can be seen in Figs. 2A and 2D, oxidation of BA starts in the double layer region, at -0.23 V, when about half of the interfacial water has been expulsed, and 0.63 V negative of the beginning of formation of the gold oxide monolayer at 0.4 V. This oxidation can only be due to the formation of highly active adsorbed OH formed at -0.23 V, Au being even more active in alkaline media than Pt [28-30]. The coverage of these OH sites is very small (the corresponding redox process appears in the CV only at higher temperatures, as shown below), but it suffices for obtaining large currents, since their hemispheric diffusion profiles overlap, and actually diffusion-limited values can be reached. A signal example of this is the oxidation of dissolved CO on Pt, in which diffusion-limited currents can be obtained at low potentials, at which only about 10% of the Pt surface is free from chemisorbed, poisoning CO [31].

At higher potentials the bidimensional gold surface oxide completely suppresses the oxidation of BA, as evidenced by the drop to nearly zero of the current after peak A2 and by the absence of current in the negative sweep until gold oxide reduction starts. In the negative sweep the sharp current increase at the beginning of peak A3 of BA oxidation (Fig.2A) exactly coincides with the sharp mass decrease of gold oxide reduction (Fig. 2D), clearly showing that BA oxidation proceeds easily on the pristine Au sites just freed from the oxide. This is typical of the oxidation of many organic compounds on noble metal electrodes, as in *e.g.* the electro-oxidation of D-mannose on Au at pH 10-13 [30].

The activity of Au for ethylene glycol oxidation is about half that for BA, although it shows no activity at all in the negative sweep. And the activity of Au for the other aliphatic alcohols, and especially for ethanol, is very low, the current in the gold oxide region being only slightly higher than that in the absence of alcohol, as can be seen in Fig. 2 and Table 1. 1- and 2-propanol show very similar CVs and mass curves, as is also the case with 1- and 2-butanol (not shown). In the negative scan aliphatic alcohols are oxidized on Au only at low scan rates, as shown for 2-propanol at 0.02 V s^{-1} in Fig. 2 I.

In Figs. 2 D→E and G→I the mass curves have been made to overlap at the reversal potential, at which, assuming that all adsorbed residues have been electrooxidized, the mass should be the same as in the buffer electrolyte. For BA oxidation the positive limit of the scan was increased slightly, because BA inhibits gold oxide formation.

Table 1. Electrochemical and mass change parameters taken from CVs and mass curves at 0.1 V s^{-1} of several alcohols on an Au/Quartz electrode at a 25 mM concentration in the pH 11 buffer

Alcohol	Onset potential V	Peak potential V	Peak current density/mA cm^{-2}	*$(\Delta m)_{min}$ μg cm^{-2}
Benzyl alcohol	-0.230	0.522	3.6	-0.03
Ethylene glycol	0.045	0.442	0.56	0.11
Ethanol	0.144	0.315	0.07	0.02
1-Propanol	0.074	0.370	0.22	0.05
2-Propanol	0.011	0.322	0.20	0.15
1-Butanol	0.077	0.404	0.19	0.01

(*):$(\Delta m)_{min} = (\Delta m_{alcohol} - \Delta m_{base})$ at the potential of the mass minimum in the positive sweep

The dependence on the alcohol concentration of the net charge of alcohol oxidation (i.e., the charge after subtraction of the charge in base electrolyte), measured from CVs at 0.1 V s^{-1}, is shown in Figs. 3A and 3B. For all the alcohols but BA the anodic charge increased linearly with the concentration, indicating that the coverage by the reactive intermediate is small, as was to be expected from the lower oxidation charges. The negative charges at low concentrations for ethanol and 2-propanol indicate that these alcohols reduce the gold oxide. The curve for BA was slightly convex, indicating a sizable coverage of the Au surface by some oxidation intermediate. We define the mass difference at the minimum, $(\Delta m)_{min}$, as the difference between the mass at the potential of the mass minimum in the positive scan in the presence of an alcohol (admitted at open circuit) and the mass in its absence, with the mass curves overlapped at the positive limit. We put forward that $(\Delta m)_{min}$ should give information on the interaction between the alcohol molecule and the electrode surface. Obviously this hypothesis is valid only if the mass at the positive potential limit is the same in the absence and presence of the alcohol, that is, if all the organic residues have been oxidized, and if the amount of gold oxide is the same. $(\Delta m)_{min}$ is negative for BA (Fig. 3C), which would mean that adsorbed BA displaces more water from the interface than its own weight. For all other alcohols $(\Delta m)_{min}$ is positive (Fig. 3C), indicating that the adsorbed aliphatic alcohols are less hydrophobic, as was to be expected, since they are either fully miscible with water (ethanol, 1- and 2-propanol, and EG) or very soluble (butanol, solubility 1.1 M). With ethylene glycol a plateau is already reached at the lowest concentration used, while for the three other alcohols the increase of $(\Delta m)_{min}$ with concentration is much smoother.

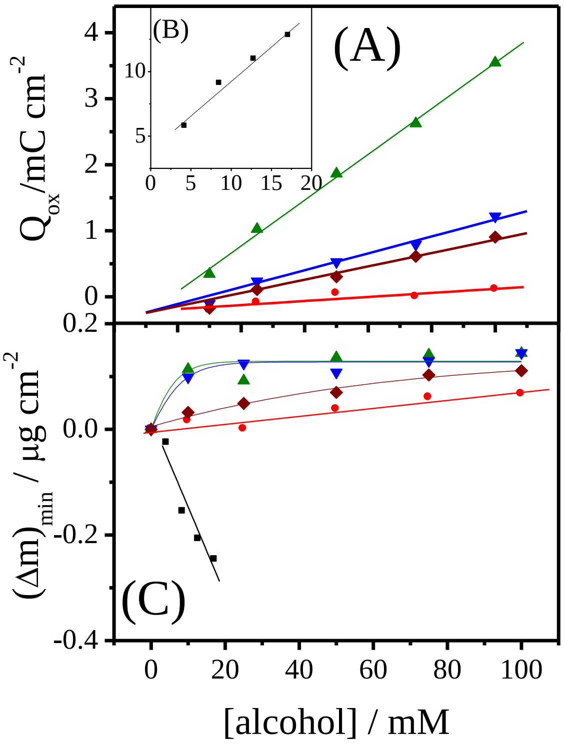

Figure 3. (A) and (B): Charge of the anodic peak of alcohol oxidation as a function of concentration for the five alcohols indicated in the inset of (C). (C): Difference, $(\Delta m)_{min,}$ between the mass at the potential of the mass minimum in the positive scan in the presence of alcohol (admitted at open circuit) and the mass in its absence, as a function of the alcohol concentration, for the same five alcohols. Data taken from Fig. 2.

It is clear that an adsorbate molecule replaces a certain number of molecules of the solvent. However, actually the mass changes should not be seen simply as due to the adsorption or desorption of species, but in terms of the coupling between the adsorbed layer and the liquid, which can change from rigid in the absence of an adsorbate to non-rigid in its presence, due to differences in the formation of hydrogen bonds [32].

3.2.2. CVs and mass curves at 0.01 V s^{-1} of benzyl alcohol and five aliphatic alcohols on Au/Q

The different behaviour of BA and the aliphatic alcohols is clearer when comparing the CV-EQCM curves at 10 mV s^{-1} of 4.3 mM BA and of 100 mM aliphatic alcohols (Fig.4) (as said above, the positive potential limit was increased for BA because it shifts positively the formation of gold oxides).

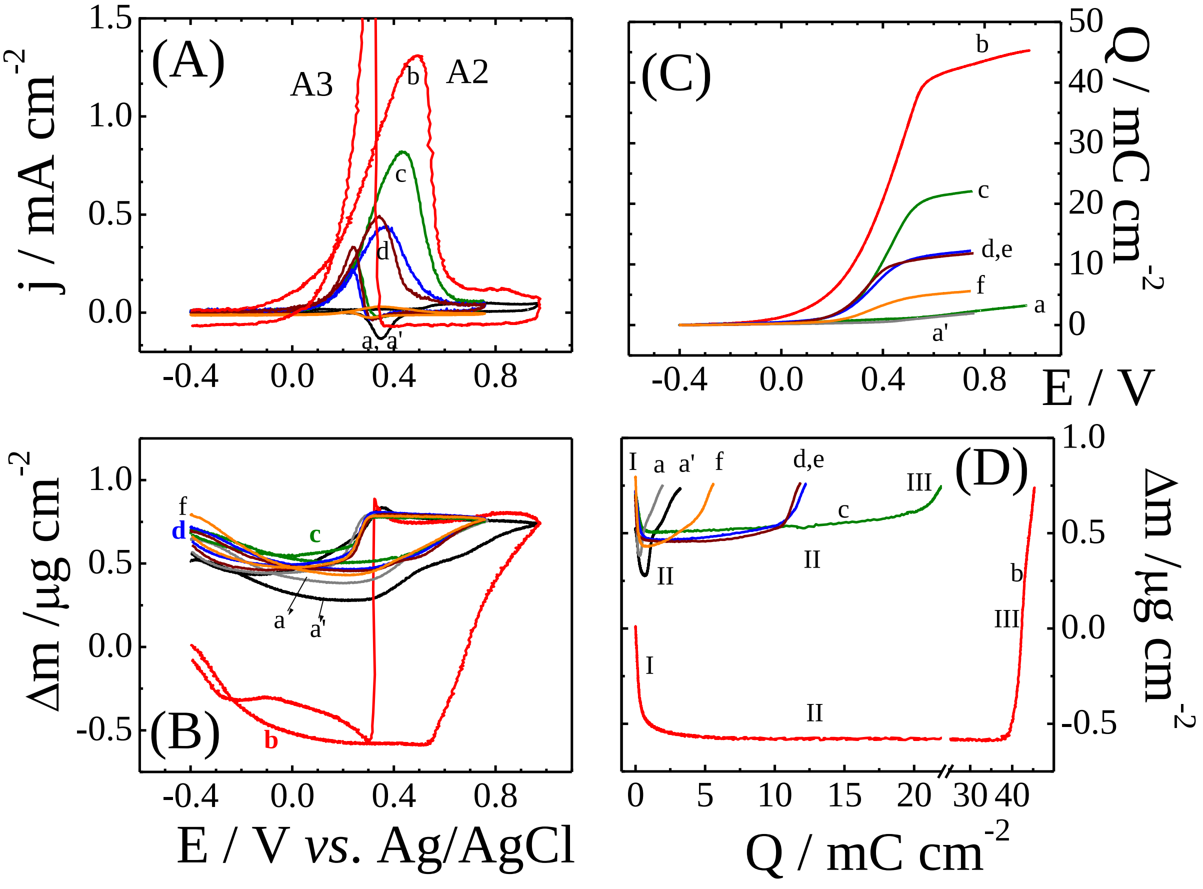

Figure 4. Comparison of the CVs and mass curves at 0.01 V s^{-1} of the Au/Q electrode in pH 11 buffer electrolyte (curves a and a') and in the presence of 4.3 mM BA (curve b), 100 mM EG (curve c), 1- and 2-propanol (curves d and e, respectively), and 100 mM ethanol (curve f). (A) Cyclic voltammograms. (B) Simultaneously recorded mass curves. (C) Electric charge obtained by integration of the CVs in (A). (D) Plot of the mass change vs. the electric charge during the positive scan.

In the positive sweep, although the concentration of BA is 23 times lower than that of the aliphatic alcohols, its oxidation peak A2 is the largest, with a peak current density of 1.3 mA cm^{-2} (Fig. 4A), about half the diffusion-limited value. For aliphatic alcohols peak A2 increases with the number of hydroxyl groups (EG, curve c) and of carbon atoms in the molecule (ethanol (curve f) < 1- and 2-propanol (curves d and e, respectively)). In the negative sweep the anodic peak A3 is again much higher for BA (curve b in Fig. 4A). Clearly peak A3 is due to the activity of pristine gold sites created by the reduction of the gold surface oxide [11, 24]. The intensity of peak A3 should be comparable with that of peak A2, and this is effectively the case, but for EG, for which peak A3 is much smaller than peak A2.

For the mass curves at 10 mV s^{-1} two reference curves in the absence of alcohol (curves *a* and *a*' in Fig. 4B), corresponding to the two positive potential limits, were used. These blank curves were made to overlap in the region of nearly constant mass after potential reversal, region 4 in Fig.1C. The curves in the presence of alcohol were overlapped with the respective blank curves at the positive limit, assuming the amount of gold oxide to be the same in the presence and absence of alcohol. Clearly, the formation of gold oxides is shifted to more positive potentials by BA (compare curve b in Fig. 4B with Fig. 1B), probably because of adsorbed residues of BA oxidation. In the negative scan the mass decrease corresponding to the reduction of gold oxides begins at the same potential for all alcohols, but in the case of BA the mass drops vertically to the same value it had at this potential in the positive scan, pointing to a rapid adsorption of BA that would displace water from the surface. For all other alcohols the mass decrease of gold oxide reduction is smooth and much smaller than that with BA.

As can be clearly seen in the plot of anodic charge vs. potential (Fig. 4C), the onset potential for oxidation is lowest (-0.1 V) for BA, higher (0.15 V) for EG (curve c) and 1- and 2-propanol (curves d and e), and highest (about 0.22 V) for ethanol (curve f). At the positive limit the charge for EG (21.7 mC cm^{-2}) is almost twice that for 1- and 2-propanol (12.2 mC cm^{-2}), and this is in turn twice that for ethanol (5.3 mC cm^{-2}). The fact that the oxidation charge is the same for 1- and 2-propanol evidences that the final products are the corresponding aldehyde (not the acid) and the ketone, respectively, with the transfer of two electrons in both cases.

As expected, a plot of the mass change in the positive scan, Δm, against the anodic charge, Q, also shows a different behavior for BA, as can be seen in Fig. 4D. Here, curve *a* corresponds to the blank for all the alcohols but BA, whose blank curve is *a*', with a higher positive limit because BA inhibits alcohol oxidation. In the presence of alcohol the minimum in the blank curve becomes the practically horizontal region II, corresponding to peak A2 of alcohol oxidation, in which the mass of the Au/electrolyte interface remains unchanged (curves b-e of Fig. 4D). In region III (gold oxidation) the large mass increase due to Au oxidation is much higher for BA because of the higher positive limit. The oxidation of BA ceases before the formation of surface gold oxides starts, and so the change between zones II and III is abrupt. On the contrary, for the aliphatic alcohols the mass increases slightly in zone II, this blurring the boundary with zone III.

The mass changes in regions I and II, the slope $d(\Delta m)/dQ$ in region III of gold oxidation, and the anodic charge in region II of alcohol oxidation, are given in Table 2. Compared with the mass decrease in region I of bare Au, that of EG is smaller, indicating that EG should be hydrophilic; those with 1- and 2-propanol are about the same as in base electrolyte; that with ethanol is 35% higher, indicating some hydrophobic character; and that of BA is more than twice higher, owing to its aromatic, highly hydrophobic character. This effect is more pronounced at low temperatures (see below).

In region II of alcohol oxidation the mass increase with ethanol is the same as in base electrolyte, with EG is about ¾, and in the presence of the propanols is about half that in their absence, indicating an increasing hydrophobic character of the respective oxidation residues. With BA the mass actually decreases in region II, unequivocally showing that its oxidation residues are highly hydrophobic. The sequence of hydrophobicity is the same as in region I, but for ethanol, which in region II shows the least hydrophobic character.

The slope d(Δm)/dQ in region III of gold oxidation is little affected by the aliphatic alcohols, and increases by 60% in the presence of BA.

Table 2. Mass changes in regions I and II, mass change per unit charge in region III of gold oxidation, and anodic charge in region II of alcohol oxidation, obtained from EQCM-CV curves at 0.01 V s^{-1} of alcohol oxidation on an Au/Q electrode in 100 mM alcohol (except in 4.3 mM for BA) in the pH 11 buffer electrolyte (from Fig. 4)

Alcohol	Δm µg cm^{-2}	Δm µg cm^{-2}	d(Δm)/dQ mg C^{-1}	Q_{II} mC cm^{-2} II
	I	II	III	
Blank (BA)	-0.235	0.195	0.16	1.89
Blank	-0.248	0.131	0.18	2.20
BA	-0.530	-0.036	0.29	34.4
EG	-0.178	0.090	0.11	17.4
1-Propanol	-0.248	0.063	0.17	8.82
2-Propanol	-0.240	0.078	0.20	9.63

3.2.3. Absence of diffusion control in the oxidation of benzyl alcohol on gold in the pH 11 buffer.

The peak current density of the oxidation of benzyl alcohol at the gold disc electrode was proportional to the square root of the scan rate up to at least 0.2 V s^{-1}, which could lead one to think that the oxidation was under diffusion control. However, the current densities of both peaks A2 and A3 *decreased* upon magnetic stirring of the electrolyte as compared with the CV under quiescent conditions, indicating that the oxidation of BA was not controlled by diffusion at all. A decrease of the current upon stirring has also been reported for the electrooxidation of propanediol on Pt and on Au in 0.1 M NaOH [33].The decrease in the current function (j_p / $v^{1/2}$) with increasing potential scan rate (v) (Fig.5) points to a reaction mechanism in which a chemical step, e.g., ionization of the alcohol yielding the alcoholate, precedes the electron transfer.

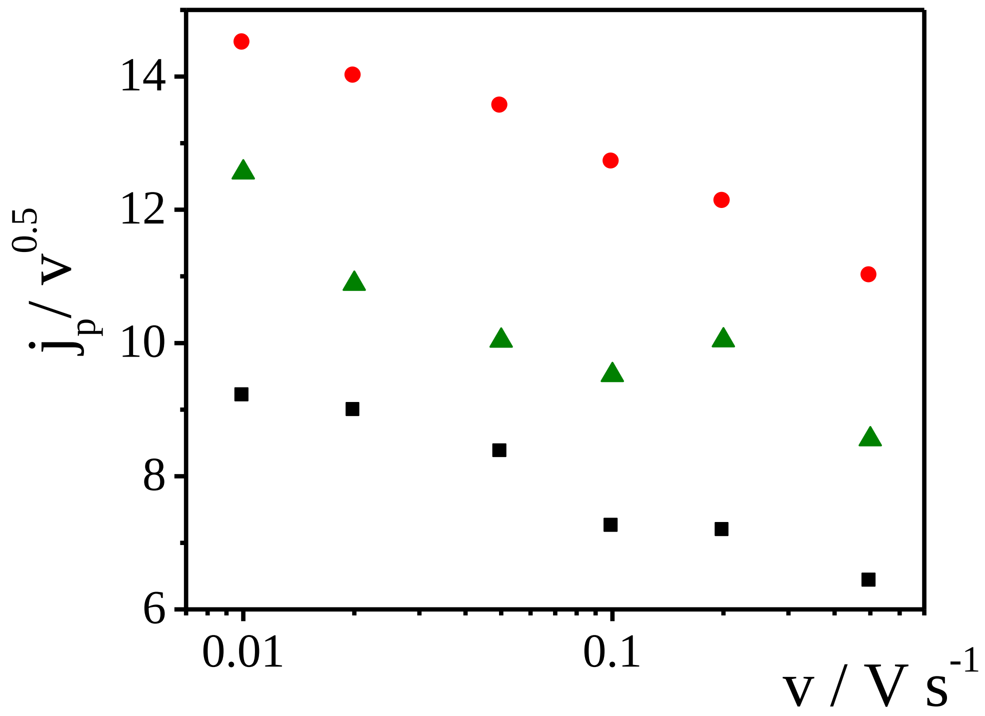

Figure 5. Current density function, j_p $v^{-1/2}$, as a function of the potential scan rate for peak A2 at pH 11, in 8,6 (■), 12.9 (▲) and 17.2 (●) mM BA.

3.2.4. Adsorption at controlled potential of benzyl alcohol and 1-propanol on Au/Q

In order to test if alcohols adsorb on Au at potentials at which their oxidation has not yet started, experiments in which the alcohol was added while the electrode was held at -0.20 V were carried out. Initially the current and mass were recorded for 10 s in order to have a reference, then the volume of alcohol required to obtain the desired alcohol concentration was injected, the solution was homogenized by nitrogen bubbling for 30 s and then left at rest for 20 s, and then a positive potential scan was started at 60 s (curves 2 and 3 for 4.3 and 23.3 mM BA, respectively, in Fig. 6A). In a blank experiment (line 1) the same volume of electrolyte was added instead. The initial masses in the background electrolyte were made to coincide (Fig. 6B). The very small, practically constant current at the initial potential was unaffected by BA addition (Figs. 6A and C). With 4.3 mM BA the mass remained constant from 40 to 60 s (curve 2 in Fig. 4B), showing that little, if any, BA is adsorbed at this concentration, while with 23.3 mM concentration (curve 3) the mass increases at 40 s by about 70 ng cm^{-2}, corresponding to at least (since the adsorption of BA would be accompanied by the desorption of water and/or ions) about 0.7 nmol cm^{-2} of BA. In agreement with this, the mass increase due to the adsorption of water and/or ions accompanying the formation of gold oxide is lowest in 23.3 mM *BA* (region III in Fig. 6B).

The potential scan provokes a steep mass decrease both in the absence and presence of BA (zones I and II in Fig.6B), which is the highest in 4.3 mM BA, and the lowest in 23.3 mM BA. Therefore, the BA adsorbed at -0.4 V at the higher concentration facilitates the expulsion of water in the subsequent sweep. Again, the potential at which gold oxidation starts, about 0.55 V, is barely affected by the presence of BA (Fig. 6C). On the contrary, the mass minimum that precedes the mass increase due to gold oxidation occurs at increasingly higher potentials with increasing BA concentration, namely, at 0.30, 0.45 and 0.60 V at 0, 4.3 and 23.3 mM *BA*, respectively, which points to the presence of an adsorbate that hinders the oxidation of gold.

The slopes (d(Δ*m*)/d*Q*) in the zone III of gold oxide formation (Fig. 6D) are 0.30, 0.39 and 0.22 mg C^{-1} in the absence of BA (line 1) and in the presence of 4.3 (line 2) and 23.3 mM BA (line 3), respectively, indicating again that only at the higher concentration does BA decrease the adsorption of water and/or ions on gold oxide. This decrease of the slope at high alcohol concentration was similar for all the alcohols studied in this work.

The potential of zero charge (pzc) of bare gold in 0.1 M NaOH is -0.09 V *vs.* SHE, and increases slightly with decreasing pH [34]. It is very interesting that when 20 mM 1-propanol is admitted at -0.4 V *vs.* Ag/AgCl (near the PZC) the mass decreases by about 0.15 μg cm^{-2} , while it does not change for adsorption potentials in the range - 0.3 V to 0 V (not shown). As is well known, the adsorption of neutral molecules is highest at the pzc, and in this case the mass increase due to the adsorption of 1-propanol is overcompensated by the concurrent expulsion of a higher mass of water from the interface.

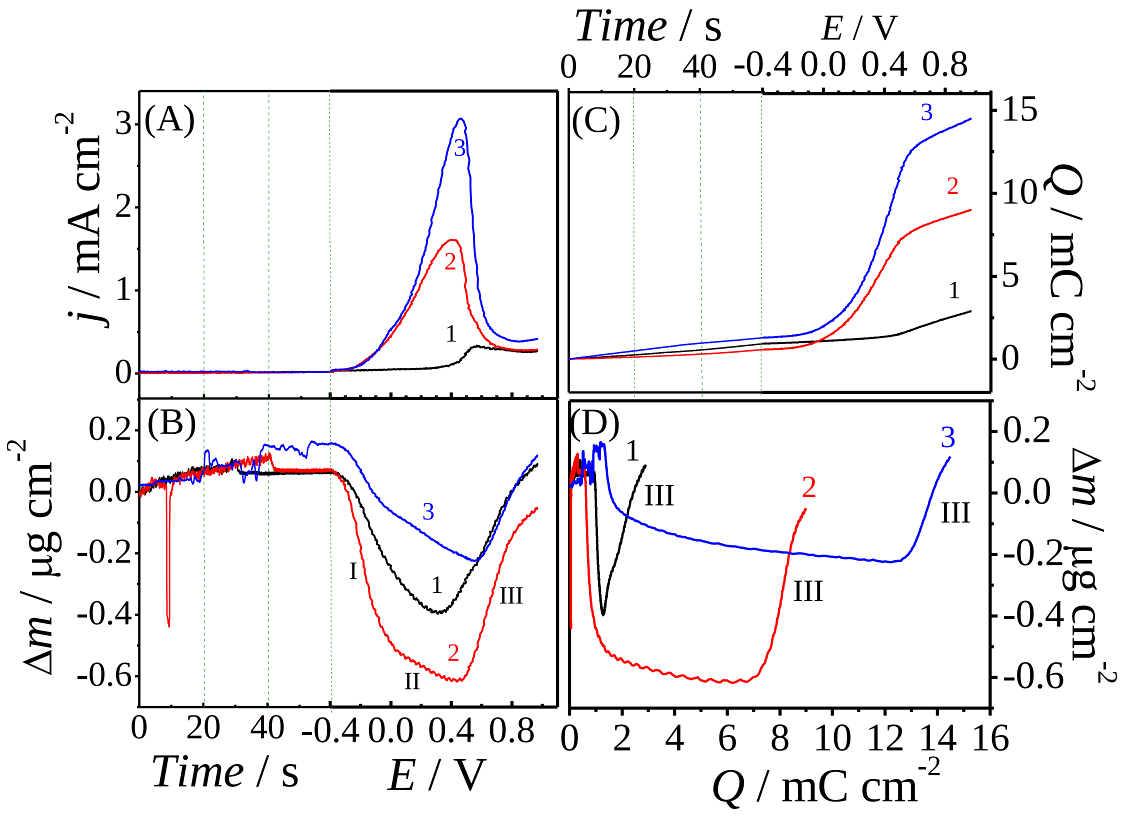

Figure 6. In this experiment an Au/Q electrode was held at -0.2 V for 10 s, then benzyl alcohol up to a concentration of 4.3 mM (curve 2) and 23.3 mM (curve 3) was added, the electrolyte was stirred by nitrogen bubbling for 30 s and then allowed to rest for 20 s, after which a linear potential sweep was started (at 60 s from beginning of the experiment). (A) Linear potential sweep in pH 11 buffer electrolyte (curve 1) and in the presence of 4.3 and 23.3 mM benzyl alcohol (curves 2 and 3, respectively). (B) Simultaneously recorded mass curves. (C) Charge integrated from plot (A). (D) Plot of mass change (Δm) vs. the charge transferred (Q) during the positive potential sweep.

3.2.5. Effect of substituents on the CVs and mass curves of benzyl alcohol on Au/Q

In order to test the effect of substituents, some experiments were carried out at 0.1 V s^{-1} in the presence of 4.3 mM and 8.6 mM of 2-methoxybenzyl alcohol and 2-chlorobenzylalcohol in 0.1 M NaOH. The results are shown in Figure 7, together with those for BA. The blank curves obtained in the absence of alcohol (thin lines) are also shown. The CVs are very similar for the three alcohols, but for a slight shift of the onset potential of 2-chlorobenzylalcohol at 4.3 mM, which is not observed at 8.6 mM.

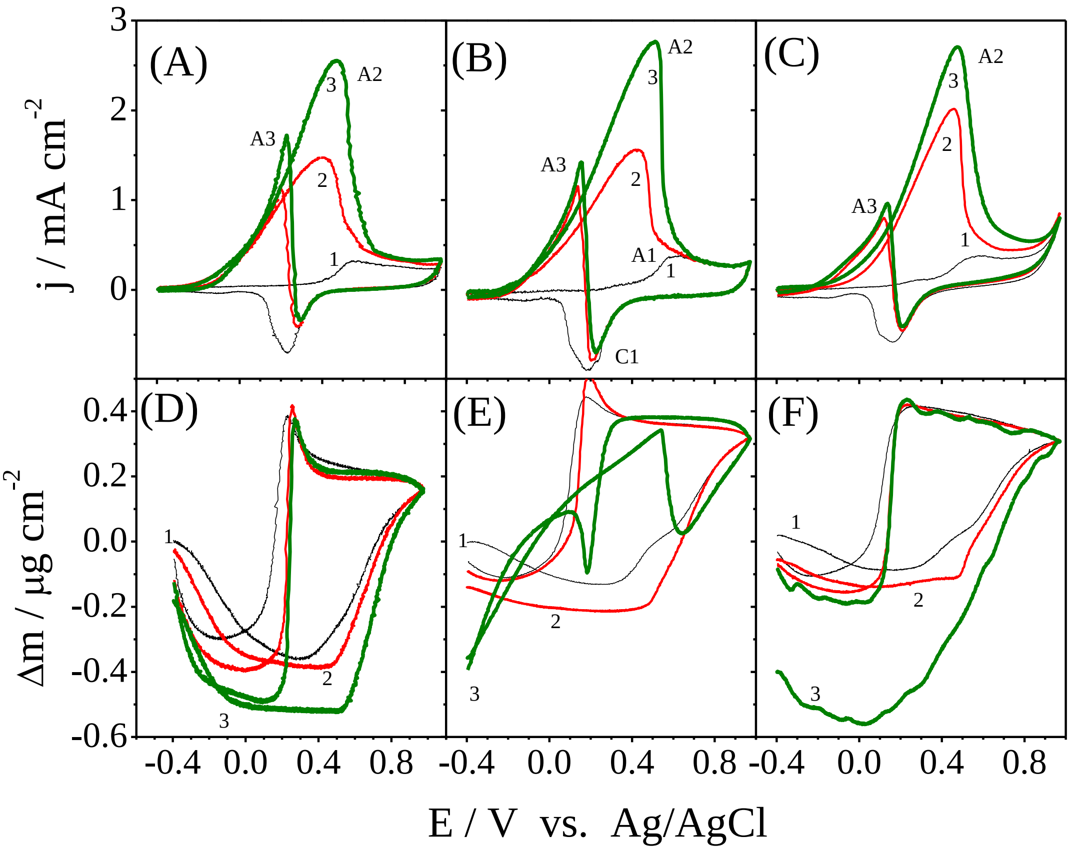

Figure 7. CVs and simultaneously recorded mass curves at 0.1 V s^{-1} of an Au/Q electrode at pH 11 (curve 1) and in the presence of 4.3 mM (curve 2) and 8.6 mM (curve 3) of: (A) benzyl alcohol, (B) 2-methoxybenzyl alcohol, and (C) 2-chlorobenzyl alcohol.

The mass change curves, which have been overlapped at the reversal potential (E_{pos}), are interesting. In 8.6 mM 2-chlorobenzylalcohol, the final mass is much lower than the initial one, to a higher degree than with BA. Probably the oxidation residues are very hydrophobic. The mass curve in 4.3 mM 2-methoxybenzyl alcohol is very similar to that of BA. However, doubling the alcohol concentration affects the mass curve to such an extent that, in order to confirm the result, the experiment was repeated, the same mass curve being obtained. The mass increases at the beginning of the scan and decreases abruptly just before gold oxidation starts, this mass decrease being equal to the mass increase in the region of the subsequent gold oxide formation. In the negative scan, the mass decrease of gold oxide reduction is not preceded by a small mass increase, occurs at a higher potential than at a 4.3 mM concentration, and is followed by a mass increase which brings the mass to about the same value as in the positive scan, the final mass coinciding with the initial one. Therefore, in spite of the dramatic change in the mass curves, most probably no residues remain on the surface.

3.3. Effect of the temperature on the CVs and mass curves of Au/Q, and of benzyl alcohol and five aliphatic alcohols, on Au/Q

The effect of temperature was studied first in the absence of alcohols. Cyclic voltammograms and mass curves at 0.02 V s^{-1} of gold/quartz electrodes in the pH 11 buffer electrolyte at temperatures from 5 ºC to 40 ºC, with an interval of 5 ºC, are given in Figs. 8A and 8B, respectively. The most important effect of increasing the temperature is the appearance of a well-defined surface redox process at -0.1 V, undoubtedly due to the adsorption-desorption of OH, in perfect agreement with the finding that the electrooxidation of BA starts at this potential (Fig. 2A). As was to be expected, the charges of gold oxide formation and reduction increase with increasing temperature, and the potential at which gold oxide formation starts decreases (Figs. 8A and 8C). The positive charge in the "double layer" region also increases with temperature (Fig. 8C), which means that in this region OH electroadsorption takes place.

The temperature dramatically affects the mass curves of Au, as can be seen in Fig. 8B, where only selected curves have been plotted to avoid cluttering. At low temperatures (5 →15 ºC) the mass curve in the negative sweep is always well above that in the positive sweep, while at 20 ºC they become much nearer to each other. At 30 ºC they cross each other at about 0.2 V, and at 40 ºC they also cross at 0.2 V, the mass at more negative potentials being much higher in the negative than in the positive sweep. It is clear that the adsorption of water on the pristine Au surface created by the reduction of the oxide decreases with increasing temperature.

The mass curves of Au/Q are shown as a function of charge in Fig. 8D. Although at the beginning of the scan the mass recording was very noisy, especially at low temperatures, it can be seen that at 5 ºC the mass increases linearly with charge over the whole positive sweep (region I of double layer, region II of beginning of OH adsorption, and region III of surface gold oxide formation, corresponding to the anodic peak in the CV). At medium temperatures (10 to 25ºC) the mass decreases in region I, remains constant in region II, and increases in region III. And at 30ºC to 40ºC, the mass decreases in both regions I and II, and then increases in region III. The mass increase of surface gold oxide formation (region III) increases with increasing temperature, but its slope, 0.14 mg C^{-1}, changes little.

The effect of temperature on the oxidation of BA, ethylene-glycol and 1-butanol on Au/Q is shown in Figs. 9, 10 and 11, respectively. As was to be expected, with increasing temperature the current in the presence of 27.3 mM BA increases over the whole CV (Fig. 9A). The mass curves at low temperatures have not been included in Fig. 9B because of their poor reproducibility.

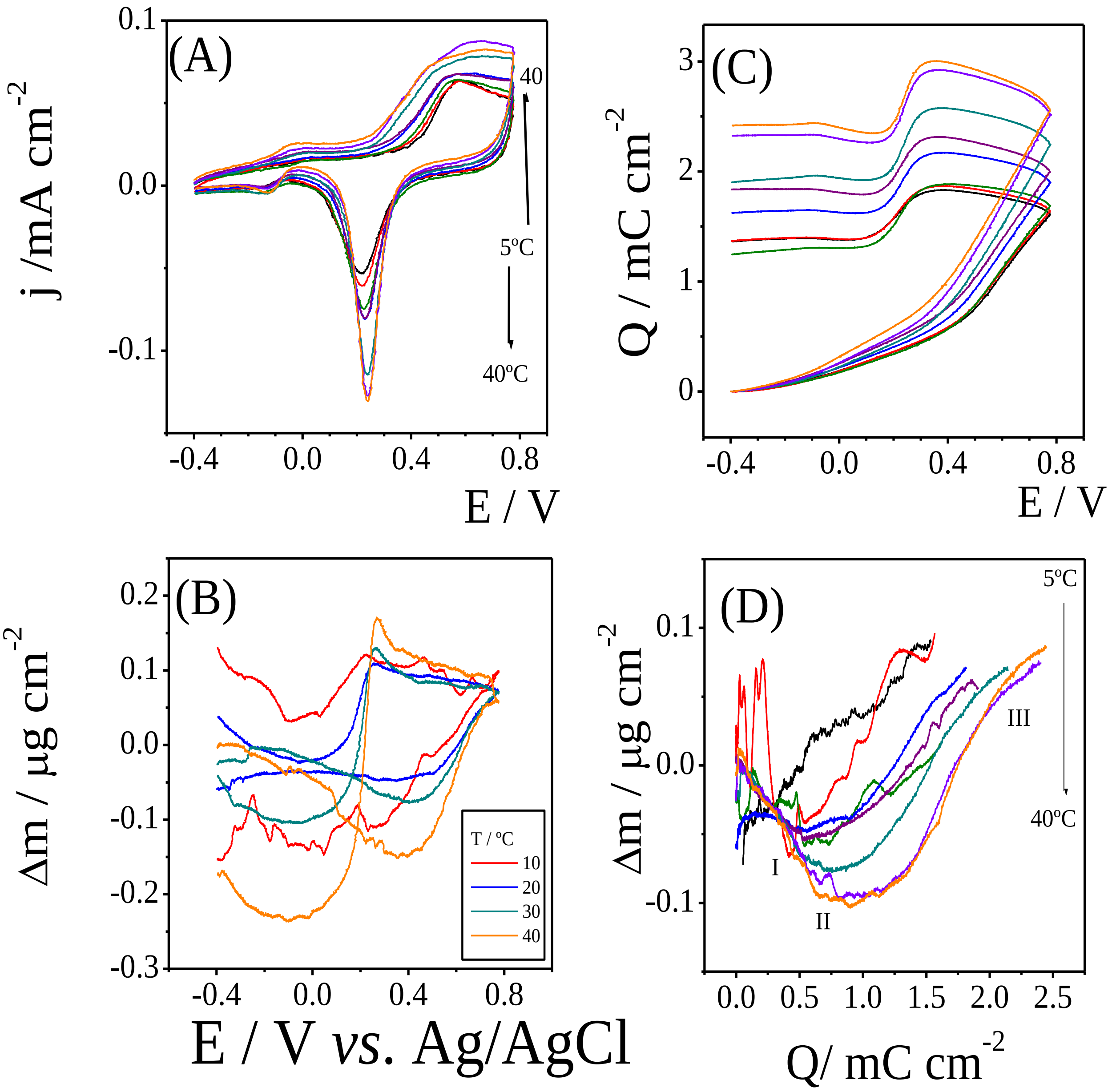

Figure 8. Influence of the temperature in the range from 5º to 40ºC on the CV and mass curve at 0.02 V s^{-1} of an Au/Q electrode in pH 11 buffer electrolyte. (A) CVs. (B) Simultaneously recorded mass curves. (C) Electric charge obtained by integration of the CVs in (A). (D) Plot of mass change (Δm) vs. the charge transferred (Q) during the positive potential sweep.

In Fig. 9B the mass curves were superimposed in the 0.4-0.6 V region of the positive potential sweep, at which assumedly BA has been expelled from the surface. The mass increase of gold oxide formation in the 0.6-0.8 V region increases with increasing temperature. The potential at which BA oxidation starts decreases markedly with increasing temperature, in agreement with the increasing formation of adsorbed OH commented above. This is more clearly seen in the plot of charge vs. potential (Fig. 9C). In the negative scan the charge remains constant, i.e., there is no oxidation, until peak A3 starts.

The mass change *vs*. charge curves in the positive sweep (Fig. 9D) show the same three regions observed with 4.3 mM BA, although in region I the mass decreases abruptly due to the higher BA concentration, 27.3 mM. In region II of BA oxidation the charge increases very much with increasing temperature, while the mass increases only slightly, so that d(Δm)/dQ is only about 1 μg C^{-1}. In region III of gold oxide formation, d(Δm)/dQ increases from 0.22 to 0.61 mg C^{-1} with increasing temperature.

Similar results to those for BA were obtained for ethylene glycol (Figure 10). Peak A2 was rather symmetrical over all the temperature range (Fig.10A), indicating a single oxidation process, which was not the case for BA (Fig. 9A). The peak current density was much smaller than that for BA, although EG has twice the number of OH groups per molecule. Consequently, the cathodic peak of gold oxide reduction can be seen in the negative sweeps.

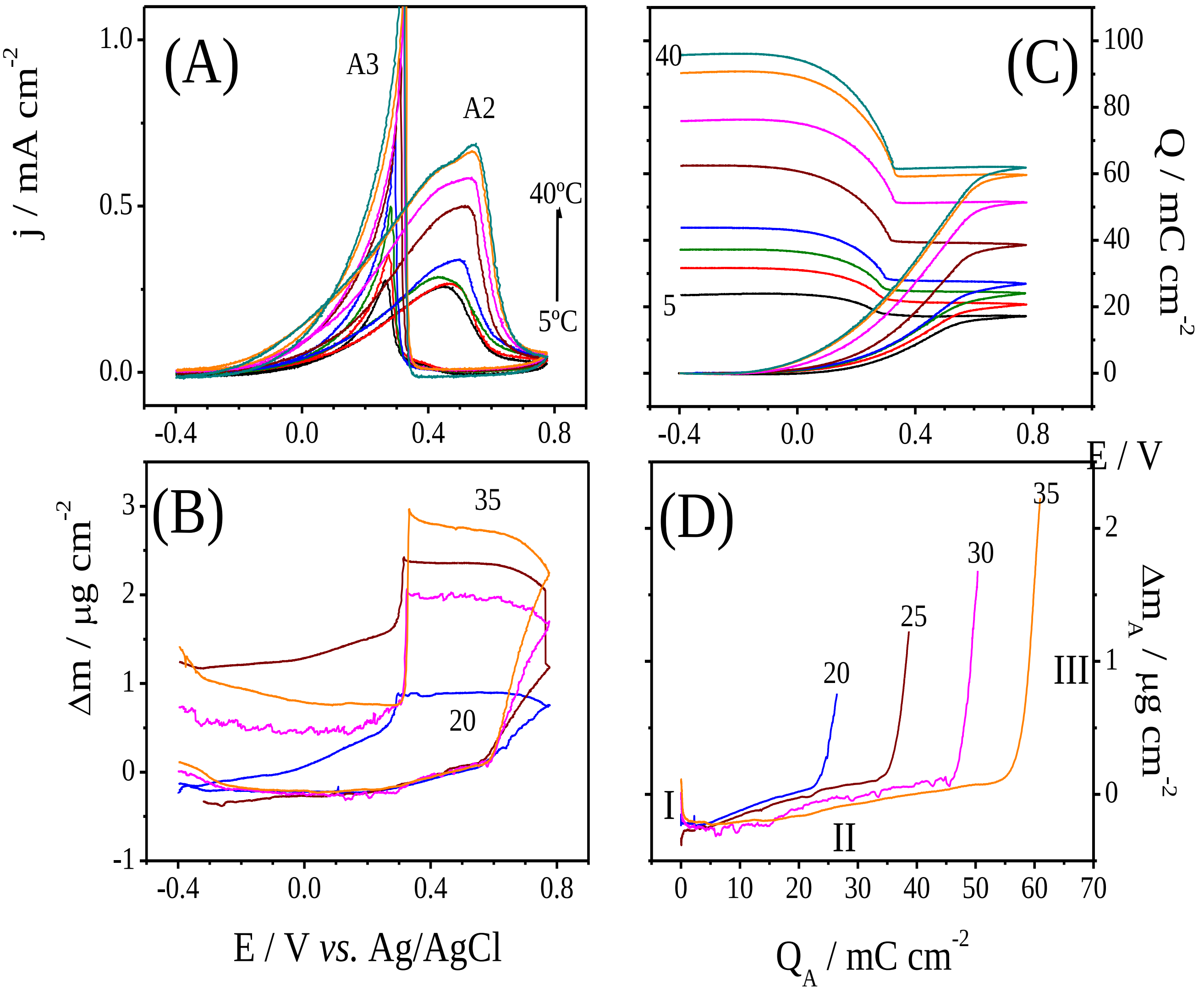

Figure 9. Influence of the temperature in the range from 5º to 40ºC on the CV and mass curve at 0.02 V s^{-1} of an Au/Q electrode in 27.3 mM benzyl alcohol in pH 11 buffer electrolyte. (A) CVs. (B) Simultaneously recorded mass curves. (C) Electric charge obtained by integration of the CVs in (A). (D) Plot of mass change (Δm) vs. the charge transferred (Q) during the positive potential sweep.

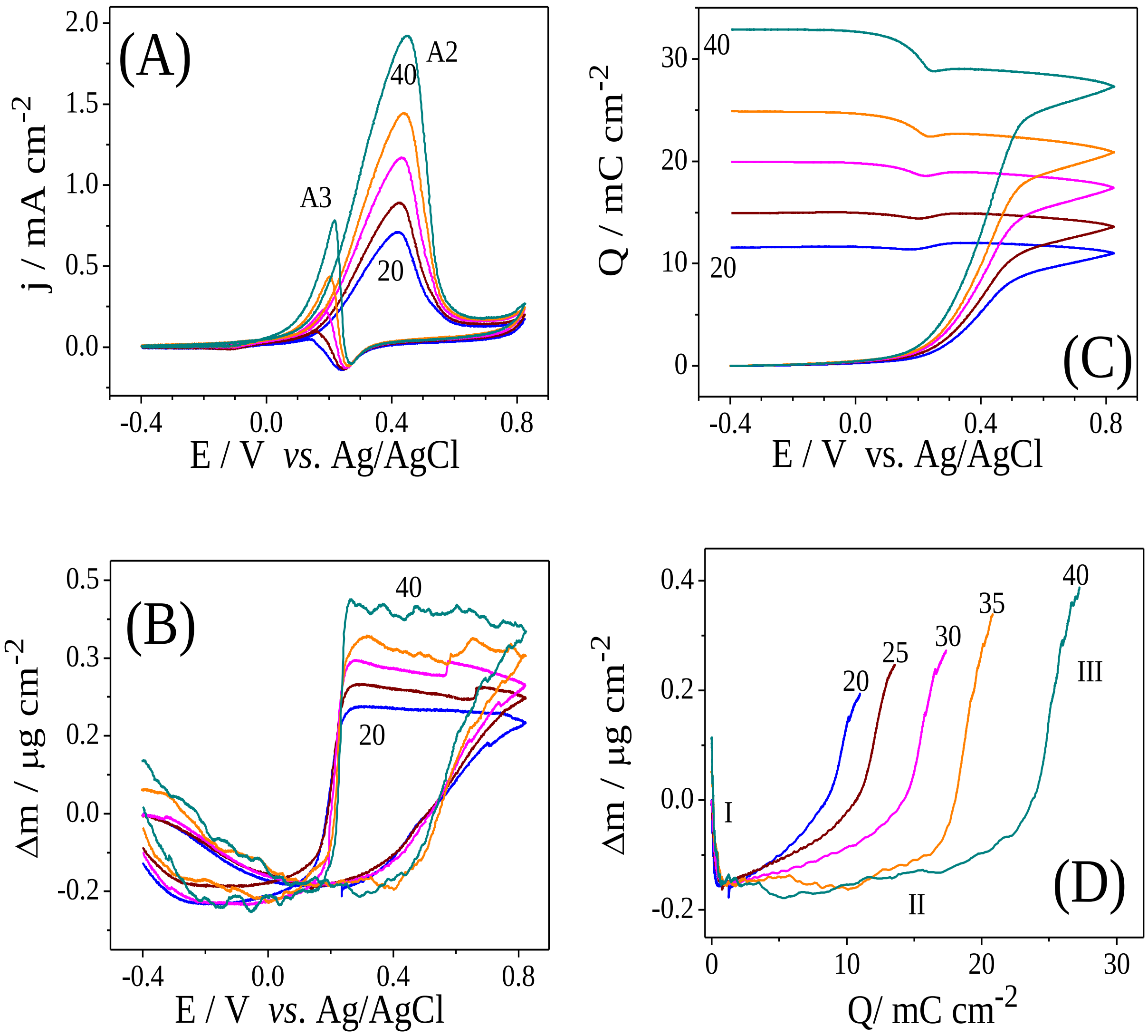

Figure 10. Influence of the temperature in the range from 5° to 40ºC on the CV and mass curve at 0.02 V s^{-1} of an Au/Q electrode in 50 mM ethylene glycol in pH 11 buffer electrolyte. (A) CVs. (B) Electric charge obtained by integration of the CVs in (A). (C) Simultaneously recorded mass curves. (D) Plot of mass change (Δm) vs. the charge transferred (Q) during the positive potential sweep.

The mass *vs*. potential curves (Fig.10B) were overlapped in the region preceding gold oxide formation, and again the mass increase due to gold oxide formation increases with increasing temperature (Fig. 10B), in agreement with the increase of the charge (Fig. 10C). The curves of charge *vs*. potential (Fig. 10C) are very similar to those of BA. On the contrary to BA, EG did not provoke large differences between the final and initial masses (Fig. 10B), showing that EG left few residues. The curves of mass *vs*. charge (Fig. 10D) show three regions, with slopes similar to those obtained in the pH 11 buffer electrolyte. The decrease of the slope at the end of Zone III, changing from 0.117 to 0.047 mg C^{-1} at 20 ºC, should be due to the beginning of oxygen evolution, as can be seen in the CV (Fig. 10A).

The results with 1- and 2-propanol are similar to those for 1-butanol, and therefore only the results for the latter are shown (Fig. 11). As with BA, with increasing temperature the current with 1-butanol increases (Fig. 11A), and the oxidation of 1-butanol begins at less positive potentials, as is more clearly appreciated in the charge vs. potential curves (Fig. 11C). The anodic peak A2 shows two processes (Fig. 11A), as is also reflected in the mass vs. charge curves, in which two slopes can be distinguished in region III of alcohol oxidation (Fig. 11D). As with BA, the mass *vs*. potential curves were overlapped at the potential just before gold oxide formation (Fig. 11B). They are little affected by temperature, indicating that 1-butanol does not alter significantly the structure of the metal/electrolyte interface.

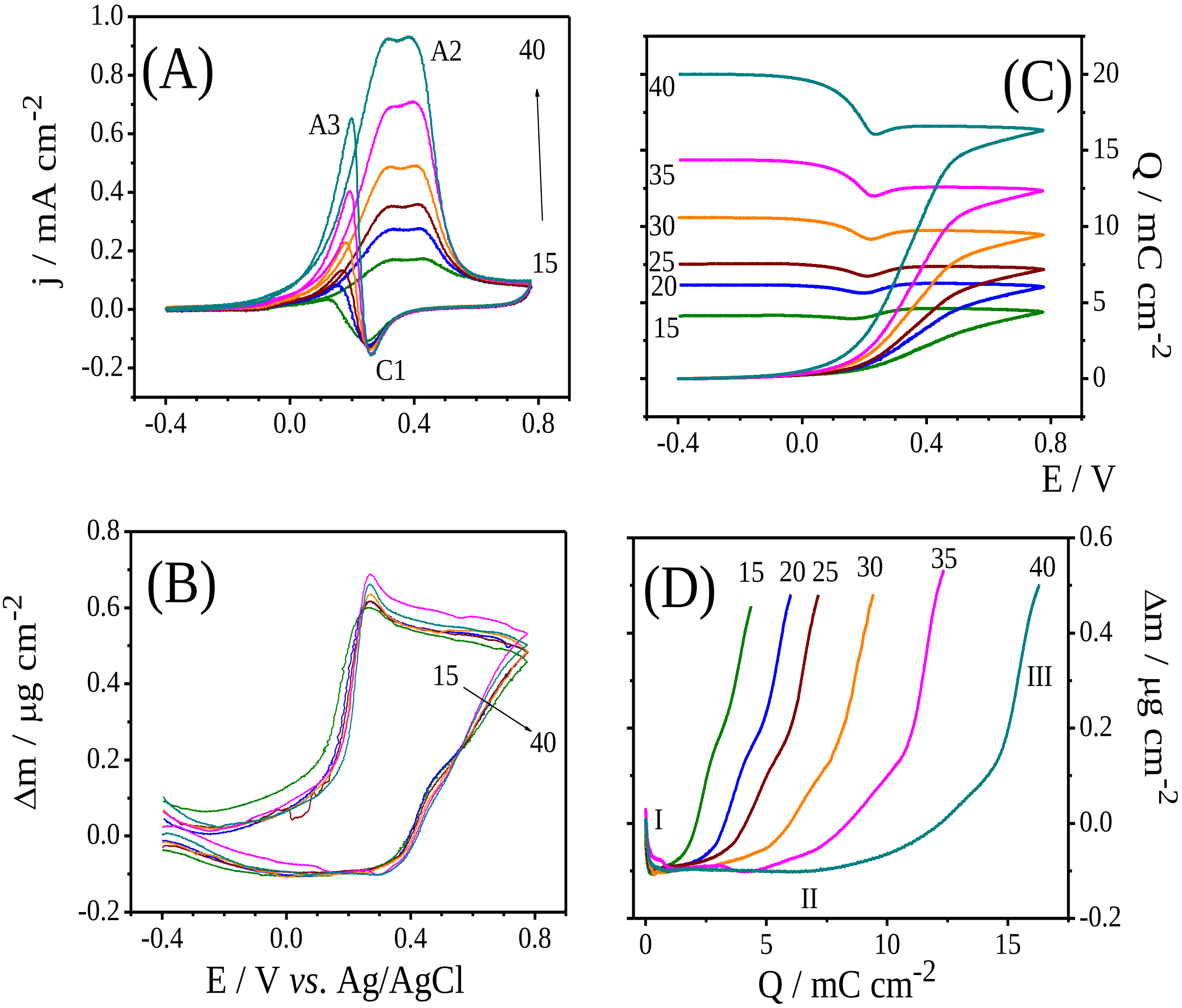

Figure 11. Influence of the temperature in the range from 5° to 40ºC on the CV and mass curve at 0.02 V s^{-1} of an Au/Q electrode in 50 mM 1-butanol in pH 11 buffer electrolyte. (A) CVs. (B) Electric charge obtained by integration of the CVs in (A). (C) Simultaneously recorded mass curves. (D) Plot of mass change (Δm) vs. the charge transferred (Q) during the positive potential sweep.

According to the Arrhenius equation for electrochemical kinetics, the apparent activation energy at a given potential *E* can be determined from the slope of a plot of the logarithm of the current density (j_E) vs. the reciprocal of the absolute temperature (1/T) [23,35]. Obviously, the current must be under exclusively kinetic control, that is, at the foot of the anodic peak. The results obtained from CVs at 0.02 V s^{-1} are shown in Figure 12 for gold in the pH 11 electrolyte in the presence of 50 mM EG (Fig. 12A) and of 50 mM 2-propanol (Fig. 12B). We could not obtain the apparent activation energies of the other alcohols because they did not yield straight lines, which is not surprising in view of the complexity of their oxidation. The estimated values of the apparent activation energy at several potentials are given in Table 3. The apparent activation energy for 2-propanol is about 50% higher than that for ethylene glycol, probably because of the presence of two OH groups in the latter facilitates its oxidation.

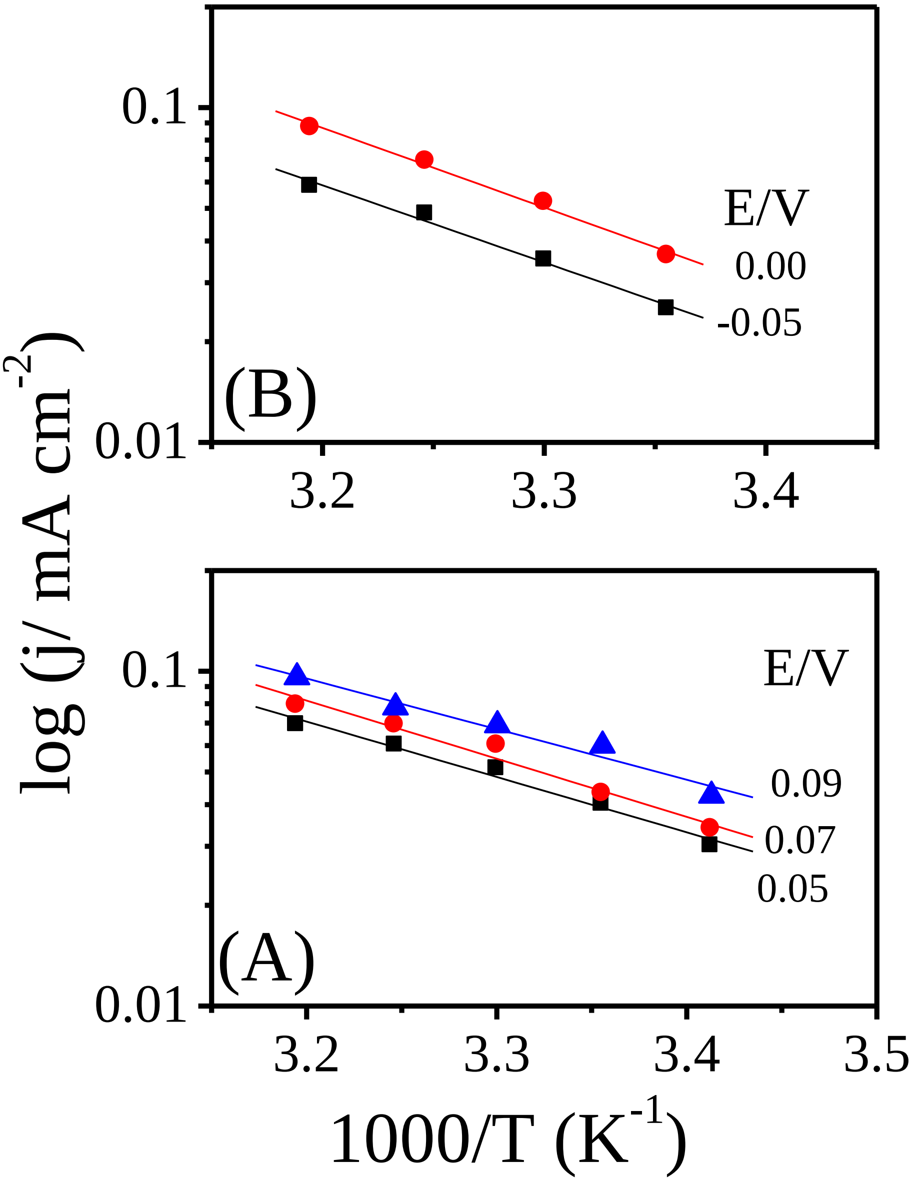

Figure 12. Arrhenius plots for the oxidation of : (A) 50 mM EG, (B) 50 mM 2-propanol, on an Au/Q electrode in the pH 11 buffer electrolyte.

Table 3. Apparent activation energy for the oxidation of ethylene glycol and 2-propanol at an Au/Quartz electrode, evaluated from plots of log j_E (from CVs at 0.02 V s^{-1}) vs. 1/T

Alcohol	Potential / V	ΔH* / kJ mol^{-1}
Ethylene glycol	0.050 0.070 0.090	27±1.7 33±3.2 29±3.1
2-Propanol	-0.050 0.000	44±3.4 45±2.9

3.4. Impedance measurements of benzyl alcohol and five aliphatic alcohols on Au

For electrochemical impedance studies a gold disc was used in a three-compartment cell, in the pH 11 buffer electrolyte and in the presence of 50 mM alcohol (1-propanol, 2-propanol, 1-butanol) and 27.3 mM benzyl alcohol. The BA concentration was lower due to its lower solubility. Three potentials were used: the first potential was the foot of peak A2 in the CV (E1), the second one was the peak potential (E2), and the third one was slightly more positive than the peak potential (E3), so that the stationary current of alcohol oxidation was minimal. Only the results for the peak potential E2 are shown in Fig. 13, because they better represent the kinetics of the system.

The impedance data were analyzed with the Randles equivalent circuit, R_u–C_{dl}//Z_f, as in previous works [36,37]. R_u is the uncompensated series resistance (about 6 Ω cm^2), and C_{dl} is the double-layer capacitance, in parallel with the faradaic impedance, Z_f, which is equal to the charge-transfer resistance, R_{ct}, plus the Warburg impedance, Z_W. The Warburg impedance gives account of the resistance to mass transfer that in the Nyquist diagrams causes a straight line of unit slope at low frequencies. NOVA 1.5 software was used; the "*electrochemical circle fit*" command for the estimation of R_{ct} made sure that the parameter *n* was close to 1.0, that is to say, that the Randles model did fit the results.

The Nyquist plots of the bare Au electrode at 0.4 V in the pH 11 electrolyte and in the presence of BA (at 0.4 V), 1-and 2-propanol (at 0.3 V) and 1-butanol (at 0.4 3V) are shown in Fig. 13A-C, the frequency region decreasing from Fig. 13A to Fig. 13C. The peak currents in the CVs were about the same for all the alcohols, which makes possible a good comparison of the impedance parameters. As the oxygen evolution was not reached, bare Au shows the beginning of a semicircle in the Nyquist plot (Fig. 12A) and only one time constant (full up triangles in Fig.13-D).

The Nyquist plots of the alcohols show a semicircle only at the respective peak potential (Fig. 13 A-C). A full semicircle, indicative of a single process [38], is observed for 1-butanol (open down triangles in Fig 13) and for BA (open stars). Only the beginning of a semicircle appears with 1-and 2-propanol. The charge-transfer resistance, R_{ct}, increases in the order BA<1-butanol<2-propanol<1-propanol, in agreement with the current densities observed in the CVs (Table 1).

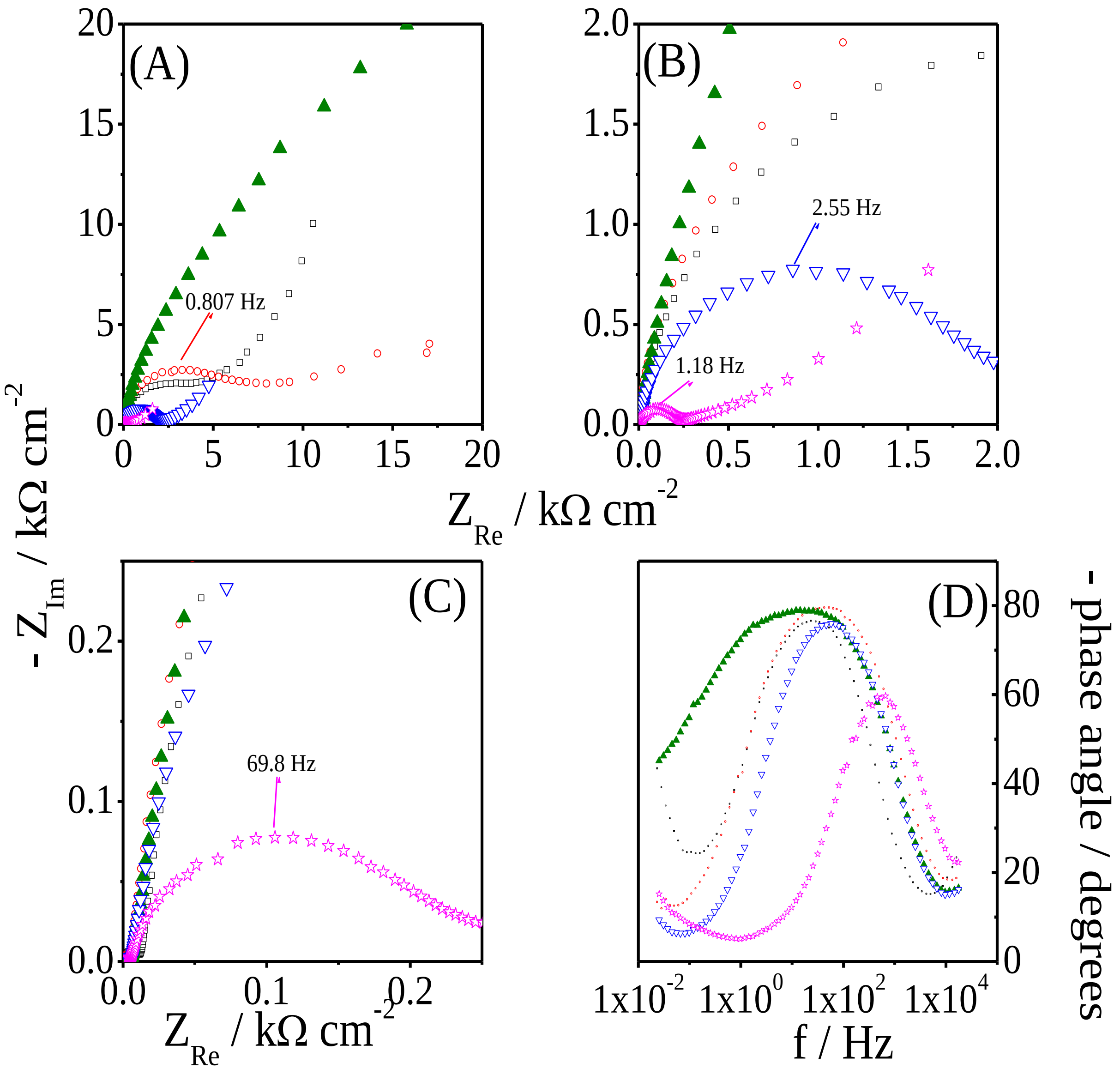

Figure 13. Nyquist plots (A, B, C) and phase angle-frequency plot (D) of a gold electrode in the pH 11 buffer electrolyte (▲, 0.4 V) and in the presence of 50 mM 2-propanol (□,0.3 V), 1-propanol (○, 0.3 V), 1-butanol (▽, 0.3 V) and 27.3 mM BA (✧, 0.25 V).

The phase angle-frequency plots (Fig13D) show a minimum at the lower frequencies, which obviously corresponds to the transition from the semicircle to a Warburg-like behaviour. The absence of a clear Warburg behaviour is probably due to a poisoning of the electrode surface by residues of alcohol oxidation. The frequency of the minimum is about 10 times higher for BA than for the aliphatic alcohols, indicating that its oxidation is more facile.

The values of R_{ct} and C_{dl} obtained from the EIS experiments are given in Table 4. The double-layer capacity with BA is about one third of that for the aliphatic alcohols, which points to an expulsion of water from the Au surface due to the hydrophobic character of BA.

Table 4. Impedance parameters for the oxidation of several alcohols at a gold disc in the pH 11 buffer electrolyte (from Fig. 13)

	R_{ct} /kΩ cm^2	C_{dl} / µF cm^{-2}
Benzyl alcohol	0.25	11.4
1-butanol	2.23	38.4
1-propanol	6.98	38.7
2-propanol	3.47	28.7

3.5. Determination of reaction products of the electrooxidaton of benzyl alcohol by HPLC

Electrolyses at controlled potential were performed in order to determine the oxidation products of benzyl alcohol oxidation. Samples of the solution taken at several times were analyzed by HPLC. The concentrations of the reaction products were evaluated using calibration curves obtained under the same experimental conditions used for the products.

The concentration of BA decreased slightly during the first 10 min and then remained constant (Fig. 14, right axis, circles). The only product detected was benzaldehyde, whose concentration increased up to a maximum of 0.058 mM, after which it decreased rapidly and then slowly (Fig. 14, left axis, squares). Therefore the initial BA concentration, 27.7 mM, remained practically unchanged. The corresponding charge obtained by integration of the I-t curve was 0.875 C at 10 min, which, assuming 2 electrons per BA molecule would yield an aldehyde concentration of 0.15 mM in the 30 mL electrolytical cell, corresponding to a faradaic efficiency for benzaldehyde formation at 10 min. of 39 %.

Evidently, a fraction of the aldehyde is oxidized to benzoic acid, which cannot be detected by HPLC, since its sensitivity for benzoic acid is 7 times smaller than that for benzaldehyde.

The oxidation products of the aliphatic alcohols could not be determined by HPLC under the experimental conditions used in this work.

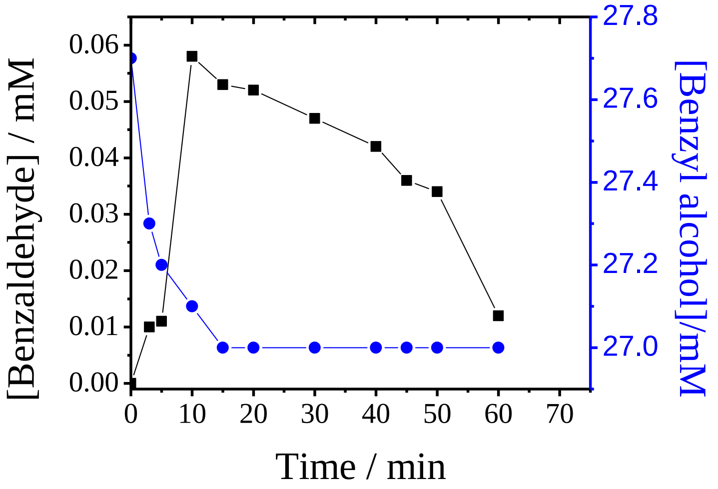

Figure 14. Concentrations of benzyl alcohol (squares, left axis) and benzaldehyde (circles, right axis) during electrolysis, determined by HPLC.

4. CONCLUSIONS

In the pH 11 buffer BA is efficiently oxidized on gold, its peak current density being almost half of the calculated diffusion-limited value. The aliphatic alcohols show much lower current densities, with the exception of ethylene glycol, its high currents probably being due to its having two OH groups.

The mass curves, and especially the lower double-layer capacity obtained from impedance measurements, suggest that the higher reactivity of benzyl alcohol is probably related to the hydrophobicity of this aromatic molecule. Its adsorption at the gold electrode would displace from the interface a higher number of water molecules than that of short aliphatic alcohols, thereby facilitating the oxidation. Experiments at constant potential with the EQCM showed that at -0.2 V the adsorption of BA on Au from a 4.3 mM solution was negligible, since the mass remained constant, but when the BA concentration was increased to 23.3 mM the mass increased by 70 ng cm^{-2}, corresponding to the adsorption of at least about 0.7 nmol cm^{-2} of BA, since its adsorption would involve the desorption of water and/or ions.

The voltammogram of BA is, but for a slight shift of the onset potential, practically unaffected by the addition of a methoxy group or a chlorine atom in position 2.

A temperature increase produced an important change in the CV of gold, namely, the appearance of a well-defined surface redox process at -0.1 V, corresponding to the adsorption-desorption of OH. It must be noted that, although at room temperature this surface process was undetectable in the CV, the electrooxidation of BA started at this potential (Fig. 2A), which unequivocally shows that it is due to reaction with this adsorbed OH.

The apparent activation energy for 2-propanol, 45 kJ mol^{-1}, is about 50% higher than that for ethylene glycol, probably because the latter has two OH groups per molecule.

ACKNOWLEDGEMENTS
The financial support of CONICYT-Chile, under Project FONDECYT 1100476, is gratefully acknowledged.

References

1. T. Iwasita, *Electrochim. Acta*, 47 (2002) 3663
2. F. Maillard, F. Gloaguen, F. Hahn and J. M. Leger, *Fuel Cells*, 2 (2002) 143
3. S. Rousseau, C. Coutanceau, C. Lamy and J.M. Léger, *J. Power Sources,* 158, (2006) 18
4. A. P. M. Camargo, B. A. F. Previdello, H. Varela and E. González, *Quim. Nova*, 33 (2010) 2143
5. E.A. Batista, G.R.P. Malpass, A.J. Motheo and T. Iwasita, *J. Electroanal. Chem*., 571 (2004) 273
6. G.A. Camara and T. Iwasita, *J. Electroanal. Chem*., 578 (2005) 315
7. V. del Colle, J. Souza-García, G. Tremiliosi-Filho, E. Herrero and J.M. Feliú, *Phys. Chem. Chem. Phy.,* 13 (2011) 12163
8. G. Tremiliosi-Filho, E. R. Gonzalez, A. J. Motheo, E. M. Belgsir, J. M. Leger and C. Lamy, *J. Electroanal. Chem*., 444 (1998) 31
9. E. Antolini and E.R. Gonzalez, *J. Power Sources*, 195 (2010) 3431
10. S. Yan, S. Zhang, Y. Lin and G. Liu, *J. Phys. Chem. C*, 115 (2011) 6986

11. M. S. Ureta-Zañartu, A. Alarcón, G. Muñoz, and C. Gutiérrez, *Electrochim. Acta*, 52 (2007) 7857
12. C. C. Jin, C. Sun, R. L. Dong and Z. D. Chen, *Electrochim. Acta*, 56 (2010) 321.
13. L. D. Burke, A. J. Ahern and A.P. O'Mullane, *Gold Bulletin*, 35 (2002) 3
14. L. D. Burke, *Gold Bulletin*, 37 (2004) 125
15. F. Gobal, Y. Valadbeigi and L.M. Kasmae, *J. Electroanal. Chem*., 650 (2011) 219
16. Z. Borkowska, A. Tymosiak-Zielinska and R. Nowakowski, Electrochim. Acta 49 (2004) 2613
17. S. C. S. Lai, S.E.F. Kleijn, F.T.Z. Öztürk, VC. van Rees V., J Koning, P. Rodriguez and MT.M. Koper, Catal. Today 141 (2010)92.
18. R. B. Kutz, B. Braunschweieg, P. Mukherjee, D. D. Dlott and A. Wieckowski, Phys Chem. Letters, 2 (2011) 2236
19. Z. X. Liang, T. S. Zhao, J. B.Xu and L. D. Zhu, *Electrochim. Acta*, 54 (2009) 2203 and references cited therein.
20. A. J. Motheo, G. Tremiliosi-Filho, E. R. González, K. B. Kokoh, J-M Léger and C. Lamy, *J. Appl. Electrochem*., 36 (2006) 1035
21. T. Vijayabarathi, K. Vijayarani and M. Noel, *Indian J. Chem. Tech*., 17 (2010) 411
22. P. S. Germain, W. G. Pell, B. E. Conway, *Electrochim. Acta*, 49 (2004) 1775 and references therein.
23. E. Gileadi, *Electrode Kinetics for Chemists, Chemical Engineers, and Materials Scientists*, VCH Publishers Inc, New York (1993), Chap. F-14.8.
24. M. S. Ureta-Zañartu, A. Alarcón, C. Berrios, G. I. Cárdenas-Jirón, J. H. Zagal and C. Gutiérrez, *J. Electroanal. Chem*., 580 (2005) 94
25. M. S. Ureta-Zañartu, C. Yáñez and J. Zagal, *Bol. Soc. Chil. Quim*., 46 (2001) 15
26. S. Bruckenstein and M. Shay, J. Electroanal. Chem., 188 (1985) 131
27. M. Tian, W.G. Pell and B. E. Conway, Electrochim. Acta 48 (2003) 2675
28. P. Ocón, C. Alonso, R. Celdrán and J. González-Velasco, *J. Electroanal. Chem*., 206 (1986) 179
29. R. R. Adzic and M. Avramov-Ivic, *J Catal.*, 101 (1986) 532
30. B. Beden, I. Cetil, A. Kahyaoglu, D. Takky and C. Lamy, *J. Catal*., 104 (1987) 37
31. J. A. Caram and C. Gutiérrez, *J. Electroanal. Chem.*, 305(1991) 259
32. L. Daikhin, E. Gileadi, V. Tsionsky, M. Urbakh, and G. Zilberman, *Electrochimica Acta*, 45 (2000) 3615
33. M. El M. Chbihi, D. Takky, F. Hahn, H. Huser, J. M. Léger and C. Lamy, *J. Electroanal. Chem.*, 463(1999) 63
34. D. D. Bodé, T. N. Andersen and H. Eyring, *J. Phys. Chem.*, 71 (1967) 792
35. E. Gileadi, *Physical Electrochemistry, Fundamentals, Techniques and Applications*, Wiley-VCH, Weinheim, (2011) p.153
36. C. Berríos, M. S. Ureta-Zañartu and C. Gutiérrez, *Electrochim. Acta*, 53 (2007) 792
37. C. Berríos, J. F. Marco, C. Gutiérrez and M. S. Ureta-Zañartu, *Electrochim. Acta*, 54 (2009) 6417
38. M. E. Orazem, B. Tribollet, *Electrochemical Impedance Spectroscopy*, John Wiley & Sons, Inc. (2008), New Jersey, Chap. 17.